JOURNAL OF SOLID STATE CHEMISTRY 39, 219–229 (1981)

Crystal Structure and Ionic Conductivity in $Na_4Zr_2Si_3O_{12}$

D. TRAN QUI, J. J. CAPPONI, AND J. C. JOUBERT

Laboratoire de Cristallographie CNRS, 166 X, 38042 Grenoble Cédex, France

AND R. D. SHANNON

Central Research and Development Department, E. I. du Pont de Nemours and Company, Experimental Station[1] Wilmington, Delaware 19898

Received December 19, 1980

Na ion conductivities of $Na_{4-x}Zr_2Si_{3-x}P_xO_{12}$ range from 3.5×10^{-4} (ohm-cm)$^{-1}$ for $x = 0$ to 1.9×10^{-1} (ohm-cm)$^{-1}$ for $x = 1.0$ at 300°C. Structure refinements of single-crystal $Na_4Zr_2Si_3O_{12}$ were carried out at 25, 300, and 620°C. Little change occurs in bond distances and angles in the $(Zr_2Si_3O_{12})^{-4}$ framework whereas the Na(1)–O_8 and Na(2)–O_8 polyhedra enlarge dramatically with increase of temperature. The large thermal motion of Na(1) and Na(2) is probably related to the Na mobility in this structure. Of the four possible Na ion pathways, only two have openings large enough to allow reasonable mobility. The first, connecting a Na(1) site to a Na(2) site, is somewhat smaller (1.86Å) than a Na ion (2.30 Å) at RT but increases substantially to 2.22 Å at 620°C. The second, connecting a Na(2) site to a Na(2) site, is larger (2.37 Å) and increases to 2.66 Å at 620°C. Difference Fournier maps show significant electron density along Na(2)–Na(2) paths and Na(2) thermal ellipsoids have major axes close to these paths.

Introduction

Ionic conductivity in compositions of the type $Na_{4-x}Zr_2Si_{3-x}P_xO_{12}$ was discovered by Hong (*1*). For the composition $Na_3Zr_2Si_2PO_{12}$ the conductivity at 300°C is comparable to the best Na β'' alumina; however, the end member $NaZr_2P_3O_{12}$ is a poor ionic conductor. The conductivity of pure $Na_4Zr_2P_3O_{12}$ at 300°C is 3.5×10^{-4} (ohm cm)$^{-1}$ and is thus only a moderately good ionic conductor in comparison with Na β'' alumina, $Na_5GdSi_4O_{12}$ (*2*) or $Na_3Zr_2Si_2PO_{12}$ (*1*). The structure of $Na_4Zr_2Si_3O_{12}$ at room temperature (RT) was determined by Sizova *et al.* (*3*). In order to gain more insight into the behavior of the mobile, partly disordered Na^+ ions in the rigid framework host $[Zr_2Si_3O_{12}]^{4-}$, the crystal structure of $Na_4Zr_2Si_3O_{12}$ was reinvestigated at RT, 300, and 620°C.

Experimental

Crystals of $Na_4Zr_2Si_3O_{12}$ were grown hydrothermally. A $\frac{3}{8} \times 5$ in. long Au tube sealed at one end was loaded with 0.5 g $K_{1.7}Na_{0.3}ZrSi_6O_{15}$ and 2 cm^3 of 50% NaOH solution. After sealing, the tube was heated to 600°C at 3000 atm external pressure, held for 24 hr and cooled slowly to RT. The resultant equidimensional crystals of $Na_4Zr_2Si_3O_{12}$, approximately 1 mm across opposite faces, were found by emission

[1] Contribution No. *2816*.

0022-4596/81/110219-11$02.00/0

spectroscopy to contain only 20–100 ppm K. Thermogravimetric analyses obtained on $Na_4Zr_2Si_3O_{12}$ crystals indicate constant weight from RT to 450°C, 1% weight loss between 450 and 650°C and constant from 650 to 1250°C. The infrared spectrum of $Na_4Zr_2Si_3O_{12}$ (Fig. 1) shows characteristic SiO_4 stretching and bending vibrations at 800–1000 and 500–600 cm^{-1} respectively (*4, 5*). Because of the absence of the characteristic vibrations of OH^- or H_2O at 3200–3600 cm^{-1} and 1600 cm^{-1}, we assume negligible quantities of OH^- and H_2O.

X-ray patterns were obtained on a Hagg–Guinier camera using $CuK\alpha_1$ radiation and a KCl internal standard (a = 6.2931 Å). Table I lists the "d" values. The cell dimensions refined by least squares from this data using space group $R\bar{3}c$ are: a = 9.1863(5) Å and c = 22.181(2) Å, V = 1621 $Å^3$, D_x = 3.383 g/cm^3, and Z = 6. It should be noted that $Na_4Zr_2Si_3O_{12}$ corresponds to phase A reported by Baussy *et al.* (*6*) in their hydrothermal study of the ZrO_2–SiO_2–Na_2O–H_2O system. Furthermore, the above cell dimensions differ greatly from those determined by Sizova *et al.* (*3*) in their determination of the structure of $Na_4Zr_2Si_3O_{12}$.

Polycrystalline samples of $Na_{4-x}Zr_2Si_{3-x}P_xO_{12}$ were prepared for conductivity measurements by solid state reaction of Na_2CO_3, Zr acetylacetonate, SiO_2 and $NH_4H_2PO_4$ at 1000°C. The conductivity samples were prepared as ½ in. diameter disks by pressing at 12,000 psi, heating for 4 hr at 1200°C and quenching in air. They were mounted in a stainless-steel holder between two disks of 0.015-in-thick Na foil,

TABLE I

POWDER DIFFRACTION DATA FOR $Na_4Zr_2Si_3O_{12}$

Index	d_{obs}	d_{calc}	I/I_0
012	6.463	6.464	25
110	4.592	4.593	90
104	4.549	4.549	90
113	3.901	3.901	50
021		3.915	
006	3.696	3.696	5
024	3.232	3.232	65
211	2.979	2.979	40
116	2.880	2.879	100
300	2.651	2.651	90
214	2.643	2.643	50
220	2.296	2.296	5
208	2.274	2.274	20
223	2.193	2.193	40
131		2.195	
217	2.181	2.181	10
306	2.155	2.154	10
10$\underline{1}$0	2.137	2.136	10
134	2.050	2.050	45
128	2.038	2.038	50
315	1.975	1.975	10
042	1.957	1.957	15
01$\underline{1}$1		1.954	
226	1.950	1.950	80
02$\underline{1}$0	1.937	1.937	25
404	1.871	1.872	5
00$\underline{1}$2	1.848	1.848	15
137	1.811	1.810	20
045		1.814	
21$\underline{1}$0	1.785	1.785	50
410	1.735	1.736	55
324	1.733	1.733	30
318	1.726	1.726	20
235	1.688	1.687	5
413		1.690	
048	1.616	1.616	5
13$\underline{1}$0	1.564	1.564	40
01$\underline{1}$4	1.553	1.553	15
33$\underline{0}$	1.530	1.531	35
054	1.529	1.529	15
238	1.524	1.524	15
30$\underline{1}$2	1.516	1.516	15

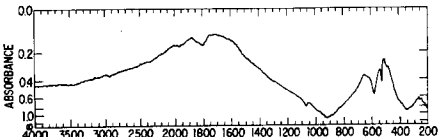

FIG. 1. Infrared spectrum of $Na_4Zr_2Si_3O_{12}$.

supported on Ni screens. The temperature was raised above the mp of Na metal to assure good contact. The ac conductance was measured from 280°C to ~75°C using a Wayne–Kerr universal bridge at a fre-

quency of 1.6×10^3 Hz. The dc conductivity was measured by applying a slowly varying voltage (a triangular wave form with a frequency less than 0.01 Hz) and recording the current. These conductivity samples had densities of ~75% of theoretical and, therefore, the conductivity values are probably low (*7*).

Table II summarizes the conductivity data and Fig. 2 shows $\sigma-1/T$ plots for the $Na_{4-x}Zr_2Si_{3-x}P_xO_{12}$ series. $Na_4Zr_2Si_3O_{12}$ has an activation energy for conduction of 8.0 kcal/mole, slightly lower than for $Na_5GdSi_4O_{12}$, the other example of a framework silicate having good ionic conductivity (*2*). Substitution of P for Si and the introduction of Na vacancies reduces the activation energy only slightly; the increase in conductivity comes primarily from the increase in the prefactor, A. The $\sigma-1/T$ plots for $Na_{4-x}Zr_2Si_{3-x}P_xO_{12}$ up to $x = 1.0$ are characterized by breaks at 200–210°C. The activation energies in the high-temperature region range from 6.1 to 6.8 kcal/mole (Table II), whereas they range from 9.1 to 10.7 kcal/mole in the low-temperature region. Similar changes in activation energy have been observed in alkali

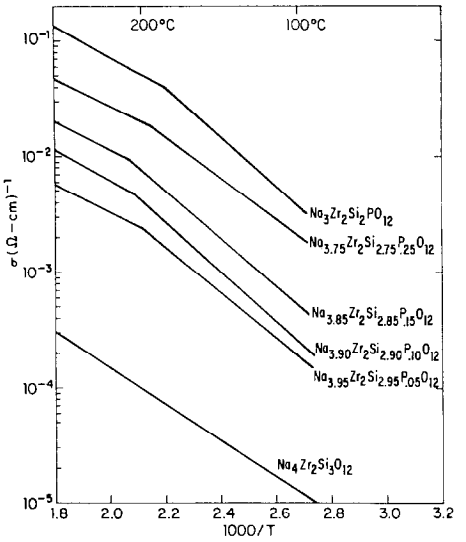

FIG. 2. $\sigma-1/T$ plots for $Na_{4-x}Zr_2Si_{3-x}P_xO_{12}$ series.

halides and are generally attributed to association of cation vacancies with impurity ions (*8*). In this case Na vacancies presumably associate with the P^{5+} ions to produce a neutral complex.

Figure 3 shows the Na^+ ion conductivity at 300°C in $Na_{4-x}Zr_2Si_{3-x}P_xO_{12}$ for $x < 1.0$. The points at $x = 0.2$ and 0.4, determined using graphite electrodes by Goodenough

TABLE II

CONDUCTIVITY DATA FOR $Na_{4-x}Xr_2Si_{3-x}P_xO_{12}$

X	E_a[a]	A	Temperature range (°C)	σ_{300}[b] (ohm-cm)$^{-1}$
0.0	8.0	2×10^2	100–270	3.5×10^{-4}
0.05	6.3	9×10^2	200–280	6.5×10^{-3}
	9.7	3×10^4	100–200	
0.10	6.8	3×10^3	210–280	1.3×10^{-2}
	10.7	2×10^5	100–210	
0.15	6.4	4×10^3	210–280	2.3×10^{-2}
	10.2	2×10^5	100–210	
0.25	6.1	6×10^3	190–280	5.3×10^{-2}
	9.1	2×10^5	100–190	
1.00	7.0	5×10^4	180–260	1.9×10^{-1}
	10.5	2×10^6	100–180	

[a] $\sigma = A/T \exp(-E_a/kT)$.

[b] Extrapolated value.

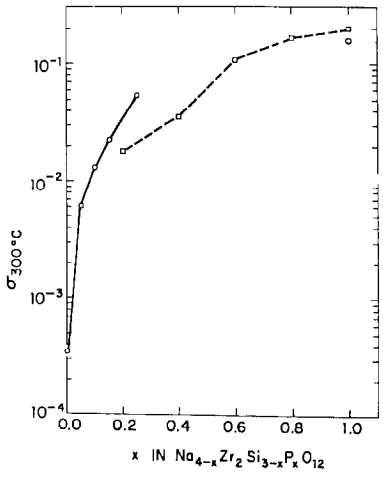

FIG. 3. Conductivity at 300°C vs x in $Na_{4-x}Zr_2Si_{3-x}P_xO_{12}$. Circles are data from this study; squares are from Goodenough *et al.* (*9*).

et al. (*9*), appear to be somewhat low. The conductivity of pure $Na_4Zr_2Si_3O_{12}$ at 300°C is 3.5×10^{-4} (ohm-cm)$^{-1}$ and is thus only a moderately good ionic conductor in comparison with Na β-Al_2O_3, $Na_5GdSi_4O_{12}$, and $Na_3Zr_2Si_2PO_{12}$ (*2*). However, as Na vacancies are introduced into the structure, the conductivity increases dramatically. We believe that the large increase in σ in primarily caused by the introduction of vacancies rather than by a change in dimensions of the lattice. Such increases in σ up to $x = 0.2$ with introduction of cation vacancies or interstitials were also noted in Li_3BO_3, Li_2CO_3, Li_4SiO_4, and Li_5AlO_4 (*7*).

X-Ray intensity data for a spherical crystal of $Na_4Zr_2Si_3O_{12}$ were collected on a computer-controlled four-circle diffractometer using Ag$K\alpha$ radiation. The crystal was heated using a hot-air device designed by Argoud and Capponi (*10*); the precision of monitored temperature was estimated to be about ±2°. The lattice constants were derived from four angular positions of 25 reflections. The intensities were collected in the ω-scan mode up to $\theta = 16°$ and in the $\theta/2\theta$ mode for higher values. The intensities of control reflections did not change significantly. Further details of the data collection are listed in Table III.

Lorentz polarization factors and spherical absorption corrections were applied to the raw data, which were finally reduced to structure amplitudes. The internal agreement between symmetry related reflections was good (Table III). At each temperature, some reflections incompatible with the *c* glide plane were observed. Because the equivalent reflections were consistent with point symmetry $3m$ and there were no significant shifts in positional parameters after refinement in $R\bar{3}$ and $R\bar{3}c$, it was assumed that these extra reflections may have been caused by multiple diffraction. A ψ-scan performed on these extra reflections confirmed the multiple-reflection phenomena. Consequently, the structure refinements were carried out in $R\bar{3}c$.

TABLE III

DETAILS OF INTENSITY MEASUREMENT AND FINAL R FACTORS

Temperature (°C)	20	300	620
Θ(max) (°C) (Ag$K\bar{\alpha}$ used)	30	30	30
Scan mode	ω-scan	ω-scan	ω-scan
Measured reflections	5961	5814	5766
Nonequivalent reflections	554	498	476
R (%)	1.9	2.6	2.6
R_w (%)	2.2	2.8	2.9

$\sigma^2 = (1/\omega)\sigma_{count}^2 [1 + 0.02 F_{ob}^2 + 0.01 F_{ob}^4]^{1/2}$

TABLE IV

POSITIONAL PARAMETERS FOR $Na_4Zr_2Si_3O_{12}$ ($\times 10^5$)

		$x(\sigma)$	$y(\sigma)$	$z(\sigma)$
Zr	RT	0	0	14679(1)
	300	0	0	14719(3)
	620	0	0	14779(2)
Na(1)	RT	0	0	0
	300	0	0	0
	620	0	0	0
Na(2)	RT	−36253(26)	0	¼
	300	−36033(43)	0	¼
	620	−35890(59)	0	¼
O(1)	RT	18532(23)	16658(26)	8488(9)
	300	18534(32)	16651(40)	8652(16)
	620	18734(41)	16685(44)	8765(17)
O(2)	RT	18458(28)	−1714(30)	19119(12)
	300	18214(49)	2102(54)	19199(20)
	620	18002(52)	−2451(55)	19206(22)
Si	RT	29683(12)	0	¼
	300	29544(14)	0	¼
	620	29486(17)	0	¼

The initial set of structure factors was calculated from positional coordinates and thermal parameters published by Sizova *et al.* (*3*). Atomic scattering factors were taken from the "International Table for X-Ray Crystallography" (*11*).

Final R factors obtained from conventional least-squares refinements (harmonic thermal motion) for the three data sets are

TABLE V

ANISOTROPIC THERMAL PARAMETERS OF $Na_4Zr_2Si_3O_{12}$ ($\times 10^4$)

		U_{11}	U_{22}	U_{33}	U_{12}	U_{13}	U_{23}
Zr	RT	52(1)	U_{11}	54(1)	$U_{11/2}$	0	0
	300	88(1)	U_{11}	93(2)	$U_{11/2}$	0	0
	630	136(1)	U_{11}	141(2)	$U_{11/2}$	0	0
Na(1)	RT	260(12)	U_{11}	80(14)	$U_{11/2}$	0	0
	300	702(32)	U_{11}	236	$U_{11/2}$	0	0
	620	1120(68)	U_{11}	223	$U_{11/2}$	0	0
Na(2)	RT	162(9)	133(9)	590(20)	$U_{22/2}$	$U_{23/2}$	97(9)
	300	368(24)	274(25)	1314(46)	$U_{22/2}$	$U_{23/2}$	255(30)
	620	543(26)	425(28)	1600(74)	$U_{22/2}$	$U_{23/2}$	356(32)
O(1)	RT	76(7)	109(9)	104(9)	129(6)	85(6)	17(7)
	300	148(12)	135(14)	201(13)	−16(8)	114(9)	82(12)
	620	213(16)	229(15)	308(18)	14(12)	82(13)	60(14)
O(2)	RT	152(9)	180(10)	216(11)	92(8)	−93(8)	8(8)
	300	278(17)	315(21)	340(17)	199(16)	−199(18)	−40(14)
	620	372(21)	518(26)	410(23)	262(19)	−181(20)	7(19)
Si	RT	52(2)	46(3)	89(4)	$U_{22/2}$	$U_{23/2}$	12(3)
	300	53(3)	77(4)	96(6)	$U_{22/2}$	$U_{23/2}$	39(5)
	620	129(4)	147(6)	189(7)	$U_{22/2}$	$U_{23/2}$	32(6)

listed in Table III. Difference Fourier analysis showed an unusual deformation of electron density around Na(2) positions suggesting the harmonic vibration model is not adequate to describe the thermal motion of Na(2) at high temperatures. Consequently, a three-dimensional anharmonic refinement using the ORJFLS program (*12*) was carried out. The positional parameters were unchanged. The thermal coefficients showed a slight departure from the harmonic model. However, the values of the third and fourth order tensors were of the same order as their SDe's, even for the data at 620°C. Thus, no interpretation of the results of this refinement was attempted.

Table IV lists the final positional parameters and Table V lists anisotropic thermal parameters. Selected bond distances are given in Table VI.

Description of the Structure

The $(Zr_2Si_3O_{12})^{4-}$ framework consists of linked SiO_4 and ZrO_6 groups. Each SiO_4 tetrahedra is linked to four ZrO_6 octahedra and each ZrO_6 octahedron is corner shared

TABLE VI

SELECTED INTERATOMIC DISTANCES IN $Na_4Zr_2Si_3O_{12}$

	RT	300	620
Zr–O(1)	2.128(2)	2.128(3)	2.131(3)
Zr–O(2)	2.034(3)	2.040(4)	2.044(5)
Na(1)–O(1)	2.489(2)	2.540(3)	2.576(3)
Na(2)–O(1)	2.571(3)	2.604(4)	2.617(7)
Na(2)–O(1)	2.5323(6)	2.519(7)	2.5180(10)
Na(2)–O(2)	2.662(2)	2.709(5)	2.735(5)
Na(2)–O(2)	3.049(3)	3.004(5)	2.971(6)
Si–O(1)	1.623(2)	1.624(4)	1.625(3)
Si–O(2)	1.625(3)	1.620(4)	1.631(5)
Na(1)–Na(2)	3.474(1)	3.495(4)	3.511(2)
O(1)–O(2)	2.707(3)	2.697(5)	2.706(5)
O(1)–O(2)	2.605(2)	2.600(4)	2.607(4)
O(1)–O(1)	2.659(3)	2.663(5)	2.660(5)
O(1)–O(2)	2.926(3)	2.920(6)	2.934(7)
O(2)–O(1)	2.901(4)	2.929(5)	2.913(6)
O(2)–O(2)	2.626(4)	2.630(6)	2.664(7)
O(2)–O(2)	3.081(4)	3.084(1)	3.085(7)
O(1)–O(1)	2.813(3)	2.822(6)	2.833(4)

with six SiO_4 tetrahedra. The mean octahedral Zr–O distance of 2.081 Å compares well with that predicted from ionic radii: 0.72 + 1.38 = 2.10 Å (*13*). The mean Si–O distance of 1.624 Å appears to be somewhat smaller than predicted from ionic radii (.26 + 1.38 = 1.64 Å) and also slightly smaller than those observed in a group of nine silicate garnets (1.641 Å) having structures similar to $Na_4Zr_2Si_3O_{12}$ (*14*).

The $(Zr_2Si_3O_{12})^{4-}$ framework contains two alkali ion sites: Na(1) is found in a six-coordinated antiprismatic site with Na–O distances of 2.489 Å and corresponds to the alkali ion position in $NaZr_2P_3O_{12}$ (*15*) and $KZr_2P_3O_{12}$. NaO_6 and ZrO_6 octahedra share faces and are arranged in triplets $O_3ZrO_3NaO_3ZrO_3$ along the *c* axis. Na(2) is found in an irregular eight-coordinate site with six oxygen neighbors at distances from 2.532 to 2.662 Å and two more distant oxygen neighbors at 3.049 Å. These sites are arranged octahedrally around Na(1) at a distance of 3.50 Å and in an approximately trigonal prismatic configuration around Na(2) at distances of 4.72 and 5.02 Å (Fig. 4). The Na(1)–O_6 and Na(2)–O_8 polyhedra share faces defined by three O(1) atoms.

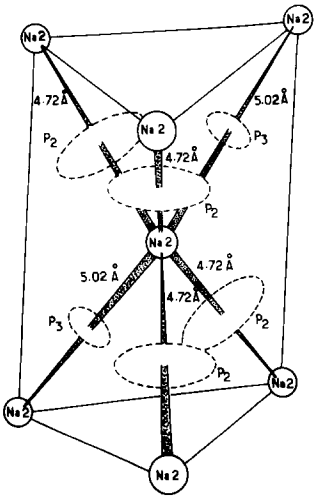

FIG. 4. Pathways between Na(2) atoms.

At 300 and 620°C very little change occurs in the $(Zr_2Si_3O_{12})^{4-}$ framework. The mean thermal expansion coefficient, α, as defined by Cameron *et al.* (*16*) is 0.52×10^{-5} °C^{-1} for the ZrO_6 octahedron and -0.33×10^{-5} °C^{-1} for the SiO_4 tetrahedron. The value for the silicon tetrahedron is similar to values found for other silicate structures (*16–18*). The value, for the ZrO_6 group is close to that predicted by Hazen and Prewitt (*19*) of 0.28×10^{-5} °C^{-1}.

The most significant changes in the structure occur in the Na–O distances and in the thermal parameters of the Na and O atoms. The mean Na(1)–O(1) distance changes dramatically with temperature (2.484, 2.540, and 2.576 Å, respectively, at RT, 300, and 620°C).

Lattice Constants and Temperature Factors

The lattice constants at different temperatures are shown in Fig. 5. The temperature dependence of c is linear whereas the a axis remains constant from RT to 620°C.

The rms D $(\langle U^2 \rangle^{1/2})$ were also computed for Na, Si, and Zr atoms. The variations of their values vs temperature (plotted in Fig. 6) are linear over the temperature range, suggesting the harmonic model for thermal vibrations still holds up to 620°C except for the Na(2) atom. Significant deviation of Na(2) component $u \parallel c$ from linear variation versus temperature suggests that at least high temperature the Na(2) thermal motion is highly hindered by oxygen neigh-

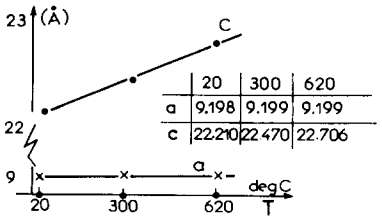

FIG. 5. Lattice constants as a function of temperature.

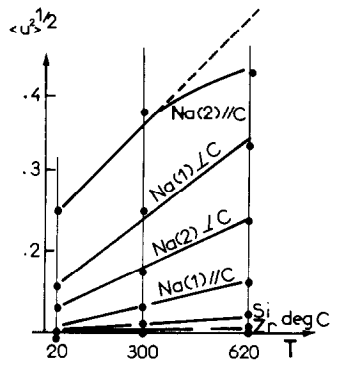

FIG. 6. Thermal root mean square displacement $\langle U^2 \rangle$ as a function of temperature.

bors. On the other hand, large thermal motion for Na(1) and Na(2) with respect to Zr and Si may be related to the high alkali ion mobilities. Constrained by $3m$ point symmetry, the Na(1) thermal ellipsoid is rotational around the c axis (Fig. 7). The rms D along this axis ($u \parallel c$) is quite small in comparison to the perpendicular component ($u \perp c$) indicating high mobility for Na(1) in the [001] plane. The Na(2) ellipsoids are oriented along a direction making an angle $\beta = 27°$ with the $Na(2)^2$–$Na(2)^4$ bond (Table VII). As the temperature increases, Na(2) ellipsoids rotate nearer to the Na(2)–Na(2) bond (the β values are respectively 25 and 23° at 300 and 620°C, suggesting preferred motion between these sites). Moreover, it is noted that Na(1) thermal amplitudes are much smaller than those of Na(2) in the temperature range 25–620°C, indicating that the potential energy for Na(1) is significantly lower than that of Na(2). These results are consistent with the fact that in $NaZr_2P_3O_{12}$ ($x = 0$) Na(1) sites were found to be completely occupied and Na(2) sites completely unoccupied.

Conductivity Paths in $Na_4Zr_2Si_3O_{12}$

Three-dimensional mobility of Na^+ ions in $Na_4Zr_2Si_3O_{12}$ depends to a large degree on the connectivity between Na sites.

TABLE VII

EQUIVALENT POSITIONS FOR Na(2)

$Na(2)^1$	$x\ 0\ \frac{1}{4}$	$Na(2)^4$	$\bar{x}\ 0\ \frac{3}{4}$
$Na(2)^2$	$0\ x\ \frac{1}{4}$	$Na(2)^5$	$0\ \bar{x}\ \frac{3}{4}$
$Na(2)^3$	$\bar{x}\ \bar{x}\ \frac{1}{4}$	$Na(2)^6$	$x\ x\ \frac{3}{4}$

There are several accessible pathways between Na atoms: one type (P_1) between Na(1) and Na(2) sites and two types (P_2 and P_3) between Na(2) sites (see Fig. 4). The relative mobility of atoms between sites should depend primarily on three factors: (1) the size of the opening through which the Na ions move, (2) the relative binding energies of the Na ions in the two different sites, and (3) a factor related to the strengths of the bonds to the O ions making up the opening. This last factor may be related to the polarizability of these bonds or to the degree of movement that these oxygen ions can undergo. The geometrical factor is the easiest to evaluate. Figure 8 shows the four types of faces shared by adjacent Na–O polyhedra. The minimum diameters D_1, D_2, D_3, D_4 of the openings along the paths P_1, P_2, P_3, P_4 (Figs. 4,8) are listed in Table VIII. D_3 and D_4 are much smaller than twice the sum of the sodium and oxygen radii; therefore, the alkali ion motion through these bottlenecks is unfavorable.

In pathway P_1, a Na(1) atom when moving to a Na(2) site passes through a triangular arrangement of O(1) atoms (pathway P_1) depicted in Fig. 8. All O(1) atoms are bonded to 1 Si, 1 Zr, 1 Na(1) and 2 Na(2) atoms and thus are the most strongly bound

TABLE VIII

MINIMUM OPENINGS IN Na–Na PATHWAYS (Å)

	D_1 Na(1)–Na(2)	D_2 Na(2)–Na(2)	D_3 Na(2)–Na(2)	D_4 Na(2)–[ ]
RT	1.86	2.37	1.18	1.56
300°C	2.00	2.46	1.18	1.58
620°C	2.22	2.66	1.18	1.58

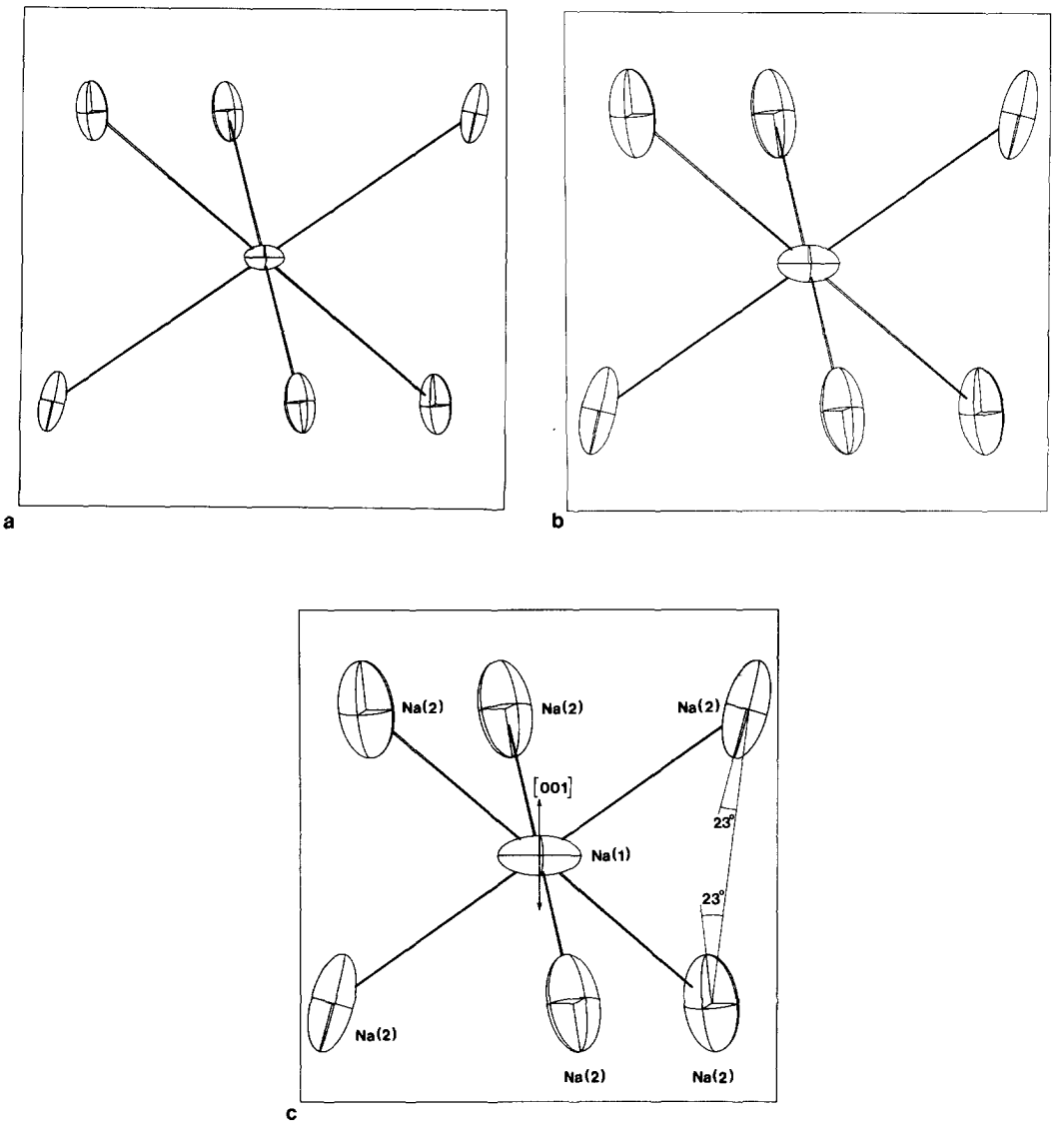

FIG. 7. Thermal vibration ellipsoids of Na(1) and Na(2) at (a) RT (20°C), (b) 300°C, and (c) 620°C.

O atoms. The minimum opening D_1 at RT described by a circle is 1.86 Å (crystal radius according to (*13*)). Although this value is somewhat smaller than the diameter of ~2.30 Å of a Na^+ ion, it is close to the RT value of 1.92 Å found in the preferred path of $Na_5YSi_4O_{12}$ (*20, 21*). The unusual increase in Na(1)–O(1) distances causes an enlargement of D_1 from 1.86 to 2.00 Å at 300°C and 2.22 Å at 620°C, and may thereby allow a significant degree of Na mobility through P_1. Although this opening is a possible pathway for Na atoms, it may not be as favorable as one of the Na(2)–Na(2) pathways, P_2. The fact that the thermal motion of Na(1) does not coincide with the orientation of P_1 is further evidence that P_1 is a less favorable channel than P_2.

There are six possible pathways between Na(2) sites. Figures 4 and 8 show the ap-

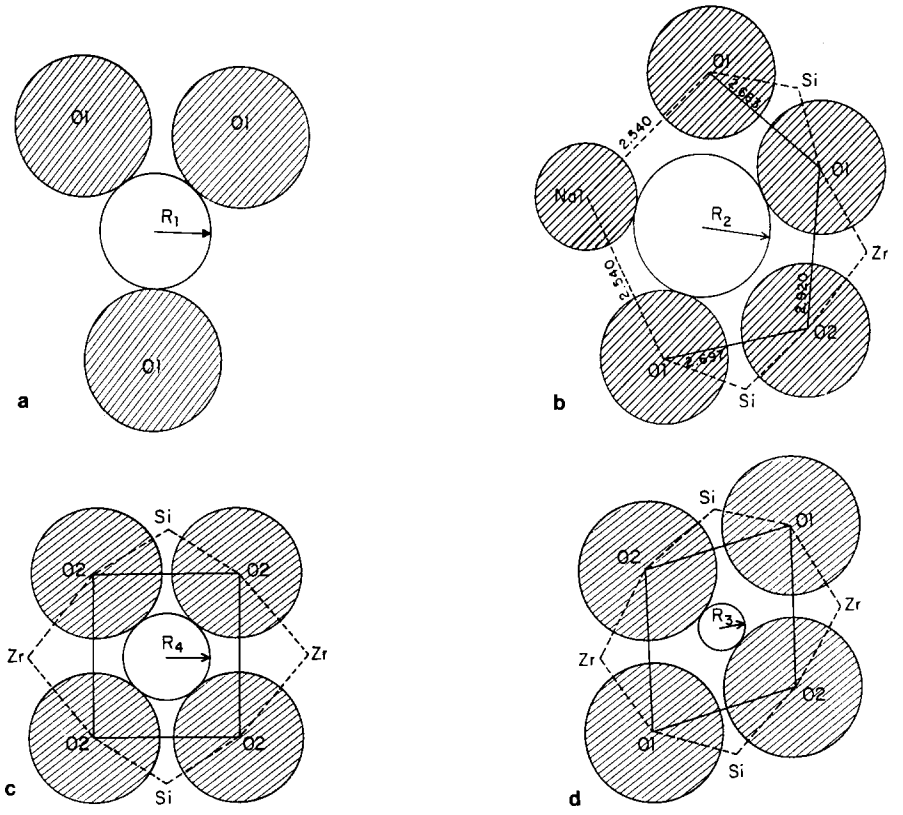

FIG. 8. Configuration of the openings in pathways: P_1: Na(1)–Na(2); P_2, P_3: Na(2)–Na(2); P_4: Na(2)– .

proximate arrangement of these pathways and the sizes of the opening between each pair of sites. The opening along P_2 is a trapezoidal arrangement of one O(2) and three O(1) atoms depicted in Fig. 8. There is also a Na(1) atom near this opening. O(2) atoms are bonded to 1 Zr, 1 Si, and 2 Na(2) atoms and thus are more weakly bonded than O(1) atoms. The minimum opening D_2 at RT described by a circle of diameter 2.37 Å is indicated in the figure. As in P_1, the increase in Na(2)–O(1) distances with temperature increases D_2 even further at higher temperatures (to 2.46 Å at 300°C). This is a very favorable path for Na(2) ions and contradicts Hong's statement "there is no passageway between Na(2) sites" in $Na_3Zr_2Si_2PO_{12}$. There are four such pathways leading from each Na(2); thus, the connectivity between Na(2) sites is favorable for 2 dimensional mobility. Indeed, the thermal motion of Na(2) atoms discussed earlier has a strong component along these directions and more closely approaches the directions of these pathways as the temperature is increased.

In order to test the preferred mobility of path P_2, difference Fourier maps defined by Na(1), Na(2)[1], and Na(2)[2] and centric equivalents were computed using the structural parameters listed in Tables 4 and 5. Such a section contains both Na(2)1–Na(2)[2]–Na(2)[4] passageways and their symmetry related passageways (see Fig. 9). The Na(2)[1]–Na(2)[2] bond shares the same oxygen O(1); therefore, motion between these sites is improbable.

Again the appearance of peaks on the 620°C map around Na(2) suggests that at HT the thermal motion of this atom was

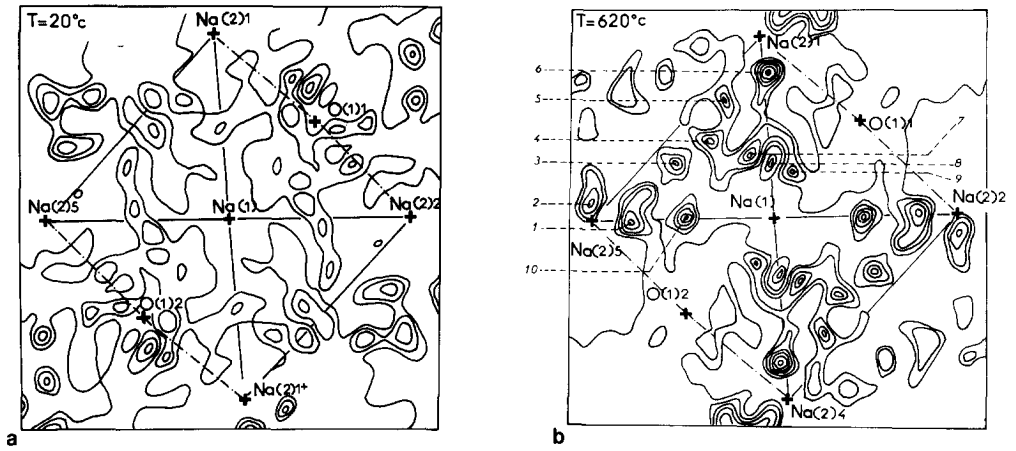

FIG. 9. Difference Fourier density section through the Na(2)–Na(2)–Na(1) plane. Full and dotted lines represent positive and negative densities, respectively. The lines are drawn at 20 intervals at arbitrary scale.

improperly described by harmonic potential.

Teardrop-like extensions of electron densities suggest two possible bent paths for Na(2) ion motion. Moving along path I (Fig. 9) should require overcoming the potential barrier induced by Zr^{4+}, thus, path II appears to be more favorable: $Na(2)^2$–$Na(2)^4$ (or $Na(2)^1$–$Na(2)^5$).

The size of the opening, although relatively easy to evaluate, may not be as important as the site preference energy. The larger thermal parameters of Na(2) relative to Na(1) and the residual electron density between Na(2) (Fig. 9) suggests that Na(2)–Na(2) exchange may be more favorable than Na(1)–Na(2), exchange despite the shorter Na(1)–Na(2) distances. This would seem to imply that Na(1) is more tightly bound than Na(2). This was discussed earlier and furthermore is consistent with bond strength arguments since Na(1) has an average Pauling bond strength of $\frac{1}{6}$ whereas Na(2) has an average bond strength of only $\frac{1}{8}$.

The third factor of some importance in determining Na motion in $Na_4Zr_2Si_3O_{12}$ may be the ease with which the opening may deform to allow passage of the Na ions. This deformation should be associated with thermal motion so that the thermal parameters of O atoms constituting the opening may be an indication of cation mobility through that opening. In the case of the Na(1)–Na(2) passageway, the O(1) atoms have significantly lower thermal parameters than O(2) atoms (see Table V). This can be associated with our observation of apparent lower mobility of the Na(1) atoms. In the case of the Na(2)–Na(2) passageway the more weakly bonded O(2) atom with its high thermal parameters may greatly augment the mobility of Na(2) atoms. The high thermal parameter of the O atom in the conductive plane of β-Al_2O_3 may also be associated with the Na mobility in that compound (*22*).

The large vibrations of Na(1) in the (001) plane suggest that a correlation could exist between Na(1) thermal vibrations and a Na jump along path P_2. Because Na(1) forms part of the D_2 opening, the Na(1)–Na(2) repulsive interaction should strongly decrease each time Na(1) moves away from the Na(2)–Na(2) path and increase when Na(1) moves back towards this path. As a

result the Na(1) thermal motion may periodically modify the potential barrier of the P_2 diffusion pathway.

The above considerations lead us to conclude that pathways P_1 and P_2 are the preferred channels for Na motion: Na–Na distances along P_1 are shorter (3.50 Å) than along P_2 (4.72 Å), but the opening D_2 is larger than D_1. The larger opening and the relatively larger thermal motion of Na(2) indicate that Na mobility in P_2 channels are higher than in P_1 channels.

Acknowledgments

We gratefully acknowledge the assistance of J. F. Whitney and C. M. Foris in obtaining the X-ray data, J. R. Barkley and N. S. Ayares for making the conductivity measurements, and N. Schlichter for obtaining the ir spectra.

References

1. H. Y.-P. Hong, *Mater. Res. Bull.* **11,** 173 (1976).
2. R. D. Shannon, B. E. Taylor, T. Gier, H.-Y. Chen, and T. Berzins, *Inorg. Chem.* **17,** 958 (1978).
3. R. G. Sizova, A. A. Voronkov, N. G. Shumyatskaya, V. V. Ilyukhin, and N. V. Belov, *Sov. Phys. Dokl.* **17,** 618 (1973).
4. P. Tarte, *in* "Proceedings, International Conference on Noncrystalline Solids," 549 (1964).
5. P. J. Launer, *Amer. Min.* **37,** 764 (1952).
6. G. Baussy, R. Caruba, A. Baumer, and G. Turco, *Bull. Soc. Fr. Mineral. Crist.* **97,** 433 (1974).
7. R. D. Shannon, B. E. Taylor, A. D. English, and T. Berzins, *Electrochim. Acta* **22,** 783 (1977).
8. R. W. Dreyfus and A. S. Nowick, *Phys. Rev.* **126,** 1367 (1962).
9. J. B. Goodenough, H. Y.-P. Hong, and J. A. Kafalas, *Mater. Res. Bull.* **11,** 203 (1976).
10. M. Argoud and J. J. Capponi, unpublished, (1977).
11. "International Tables for X-ray Crystallography," Vol. IV, pp. 155 and 316. Birmingham: Kynoch Press (1974).
12. C. K. Johnson, *in* "Thermal Neutron Diffraction" (B. T. M. Willis, Ed.), p. 132. Oxford Press, Oxford (1970).
13. R. D. Shannon, *Acta Crystallogr. Sect.* **32,** 751 (1976).
14. G. A. Novak and G. V. Gibbs, *Amer. Mineral.* **56,** 791 (1971).
15. L. Hagman and P. Kierkegaard, *Acta Chem. Scand.* **22,** 1822 (1968).
16. M. Cameron, S. Sueno, C. T. Prewitt, and J. J. Papike, *Amer. Mineral.* **58,** 594 (1973).
17. G. E. Brown and C. T. Prewitt, *Amer. Mineral.* **58,** 577 (1973).
18. S. Sueno, M. Cameron, J. J. Papike, and C. T. Prewitt, *Amer. Mineral.* **58,** 649 (1973).
19. R. M. Hazen and C. T. Prewitt, *Amer. Mineral.* **62,** 309 (1977).
20. H. U. Beyeler, R. D. Shannon, and H.-Y. Chen, to be published.
21. H.-Y. Chen, T. E. Gier, and R. D. Shannon, to be published.
22. A. W. Sleight, J. E. Gulley, and T. Berzins, Advances in Chemistry Series, No. 163, "Solid State Chemistry of Energy Conversion and Storage," p. 195. Amer. Chem. Soc., Washington, D.C. (1977).